

---

# Towards Quantifying Long-Range Interactions in Graph Machine Learning: a Large Graph Dataset and a Measurement

---

Huidong Liang\* Haitz Sáez de Ocariz Borde\* Baskaran Sripathmanathan\*  
 Michael Bronstein Xiaowen Dong

University of Oxford

## Abstract

Long-range dependencies are critical for effective graph representation learning, yet most existing datasets focus on small graphs tailored to inductive tasks, offering limited insight into long-range interactions. Current evaluations primarily compare models employing global attention (e.g., graph transformers) with those using local neighborhood aggregation (e.g., message-passing neural networks) without a direct measurement of long-range dependency. In this work, we introduce *City-Networks*, a novel large-scale transductive learning dataset derived from real-world city roads. This dataset features graphs with over  $10^5$  nodes and significantly larger diameters than those in existing benchmarks, naturally embodying long-range information. We annotate the graphs using an eccentricity-based approach, ensuring that the classification task inherently requires information from distant nodes. Furthermore, we propose a model-agnostic measurement based on the Jacobians of neighbors from distant hops, offering a principled quantification of long-range dependencies. Finally, we provide theoretical justifications for both our dataset design and the proposed measurement—particularly by focusing on over-smoothing and influence score dilution—which establishes a robust foundation for further exploration of long-range interactions in graph neural networks.

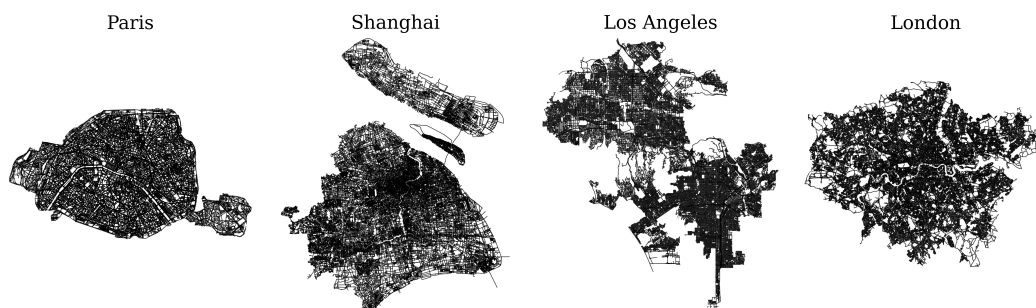


Figure 1: Visualizations of *City-Networks* for Paris, Shanghai, Los Angeles, and London.

## 1 Introduction

Graphs are a widely used mathematical abstraction across nearly every branch of science. They are particularly effective for modeling the intricate and non-uniform interactions found in real-world data, where nodes stand in for objects and edges depict their connections. The growing recognition of the versatility of graph representations has sparked intense interest in Graph Neural Networks

---

\*Equal contribution.

(GNNs) (Scarselli et al., 2009), driving innovation in deep learning for both geometric and graph-centric applications. Most GNNs exchange information between one-hop neighbors per layer to build node representations, hindering their ability to model long-range interactions. Indeed, the majority of GNN architectures have remained shallow compared to their counterparts in the Large Language Model (LLM) and Computer Vision (CV) literature, arguably due to the *small world* effect (Watts & Strogatz, 1998) observed in most citation and social networks (Yang et al., 2016b), which have traditionally been the focus of graph representation learning research. Generally speaking, despite comprising thousands of nodes, such networks have short average path lengths and high clustering coefficients, making it possible to process a high proportion of the network with only a few message-passing layers.

To better understand long-range interactions, recent efforts, such as the Long Range Graph Benchmark (LRGB) (Dwivedi et al., 2023), have introduced alternative graph datasets. However, two significant challenges remain. First, the LRGB datasets focus on inductive learning tasks with relatively small graphs of around 500 nodes, while currently there is no benchmark for long-range dependencies on large graphs for transductive learning in the literature. This is a critical gap since applying standard Graph Transformers, which are expected to better capture long-range interactions, to large graphs is significantly more challenging compared to small-graph inductive learning tasks due to the computational complexity of global attention (Borde, 2024). Second, to justify the long-range dependencies in their datasets, the authors of LRGB primarily focused on comparing classical GNNs with Graph Transformers, where they empirically observed performance gaps which are then associated with the capability of long-range signal handling. However, conclusions that are solely derived from comparisons of downstream performance gaps may not be reliable as they can be largely influenced by hyperparameter tuning as shown in Tönshoff et al. (2023), leading to an ambiguous assessment of the long-range interactions.

To address these limitations, we propose *City-Networks*, a transductive learning dataset based on large-scale city road networks with long-range annotations, and introduce a measurement to quantify long-range dependency. We then provide theoretical justification of both. Our contributions can be summarized as follows:

- Our dataset consists of four city road networks with a topology distinct from those commonly found in the literature. In particular, it features grid-like large graphs with up to  $500k$  nodes and diameters of up to 400, where the node labels are annotated based on an approximation of eccentricity, which inherently requires long-range dependency for its calculation. To the best of our knowledge, this is the first large-graph dataset designed for testing long-range dependencies in graph representation learning.
- We design a methodology to empirically test classical GNNs and Graph Transformers on our dataset by varying the number of model layers and sampled neighborhood hops. The results show that communication with neighbors from distant hops consistently improves the performance of all models, supporting the presence of long-range signals in our dataset.
- To quantify such long-range dependency, we further introduce a model-agnostic measurement that considers the per-hop influence of a given node’s neighbors on its prediction, which is estimated by the aggregated  $\ell_1$ -norm of the Jacobian from a trained model at each hop around the given node. Interestingly but not surprisingly, we observe that distant hops exert a greater influence on our *City-Networks* compared to other social networks in the transductive learning literature.
- We theoretically justify the graph structure in our dataset from a spectral perspective on over-smoothing, whose rate we link to the algebraic connectivity and diameter of the graph. Similarly, we relate our proposed measurement to the concept of influence as defined in the literature and study the dilution of mean influence score in grid-like graphs.

## 2 Datasets: City Road Networks

As shown in Figure 1, our proposed *City-Networks* is based on street maps of four cities<sup>2</sup>—Paris, Shanghai, Los Angeles, and London, which are obtained by querying OpenStreetMap (Haklay & Weber, 2008) with OSMnx (Boeing, 2024). In the following sections, we first compare the characteristics of our proposed networks with existing benchmarks, and then discuss the construction of node

---

<sup>2</sup>Code for reproducing our dataset and experiments can be found at [github.com/LeonResearch/City-Networks](https://github.com/LeonResearch/City-Networks).

Table 1: Summary statistics of our City-Networks compared to LRGB, Planetoid, and OGB.

Dataset Statistics	City-Networks (ours)				LRGB		Planetoid		OGB
	Paris	Shanghai	L.A.	London	PascalVOC	COCO	Cora	CiteSeer	ogbn-arxiv
# Nodes	114k	184k	241k	569k	479	477	2.7k	3.3k	169k
# Edges	183k	263k	343k	759k	1.3k	1.3k	5.3k	4.6k	1.16m
Avg. degree	3.2	2.9	2.8	2.7	5.7	5.6	3.9	2.7	13.7
Std. degree	0.8	1.0	1.0	1.0	1.2	1.2	5.2	3.4	68.6
Max. degree	15	8	9	10	10	10	168	99	13k
Avg. cluster coef.	0.03	0.04	0.04	0.04	0.43	0.43	0.24	0.14	0.23
Transitivity	0.03	0.04	0.05	0.05	0.40	0.40	0.09	0.13	0.02
Diameter est.	121	123	171	404	28	27	19	28	25
Node homophily	0.70	0.75	0.75	0.76	0.92	0.90	0.81	0.73	0.65

features and labels in detail, after which we provide a task description with intuitive visualizations and explanations. Readers are also referred to Appendix A for more details regarding our dataset.

**Network statistics.** We consider a city network inclusive of all types of roads in the city (e.g., *drive, bike, walk, etc.*), where nodes in the graph represent road junctions, and edges represent the road segments. After obtaining the raw data, we post-process the city networks by 1) making the graphs undirected so that they only represent connectivity between junctions (see Appendix A for details); 2) retaining the largest connected component in each city and summarize their network statistics in Table 1. Compared to citation networks from Planetoid (Yang et al., 2016a) and OGB (Hu et al., 2020), our city networks exhibit much lower maximum and average degrees with low standard deviations. At the same time, they have much larger diameters with minimum estimation ranging from 100 to 400, whereas the citation networks typically have diameters of around 20 to 30. Compared to super-pixel graphs from LRGB<sup>3</sup>, our city networks have a much larger graph size of more than  $10^5$  nodes with large diameters, and meanwhile maintain a relatively low clustering coefficient and transitivity. We refer readers to Appendix A.1 for a more detailed explanation of these statistics and our estimation methods.

**Real-world node features.** The node features in our dataset are derived from real-world features provided by OpenStreetMap for both road junctions and road segments. Specifically, the original node features consist of *longitude* and *latitude* of the road junction, the adjacent *road count*, as well as type of land use at the coordinate (e.g., *residential, industrial, forest, etc.*). For edge features, real-valued features like *road length* and *speed limit* are available, as well as binary features like *one-way* and *reversed* and categorical features such as road types (e.g., *primary, service, residential, etc.*). After one-hot encoding binary and categorical features, we obtain a total of 12 node features and 25 edge features. Next, we apply a simple neighborhood aggregation that transfers edge features to node features by averaging the features of incidental edges and then concatenating them to the features of the focal node. These new node features represent, for instance, the average speed limit around a road junction or the probability of finding a residential road nearby. As a result, the final dataset contains 37 node features after processing, where the original edge attributes are then discarded.

**Node labels based on eccentricity.** To create class labels that require long-range dependency, we compute an approximation of eccentricity  $\varepsilon(v)$  in network science (Newman, 2018), which measures the maximum distance from a node  $v$  to all other nodes in the graph  $\mathcal{G} = (V, E)$  by the following expressions:

$$\varepsilon(v) = \max_{u \in V} \rho_w(v, u), \quad \rho_w(v, u) = \min_{\pi \in P(v, u)} \sum_{e \in \pi} w(e), \quad (1)$$

where  $\rho_w(v, u)$  is the weighted shortest path distance from node  $v$  to node  $u$ ,  $P(v, u)$  is the set of all possible paths from node  $v$  to node  $u$ , and  $w(e)$  denotes the edge weight (we use road length here) for edge  $e$ . However, obtaining  $\varepsilon(v)$  for all nodes  $v \in V$  requires computing all pair-wise shortest paths in the network, which has a computational complexity of  $\mathcal{O}(|V|^3)$  using the Floyd-Warshall algorithm (Floyd, 1962) hence prohibitively expensive for our large-scale networks. Instead of focusing on the entire graph, for each node  $v$ , we only consider its 16-hop neighborhood, that is, an

<sup>3</sup>In the case of LRGB each dataset has multiple graphs; we compute average statistics for 1,000 samples.

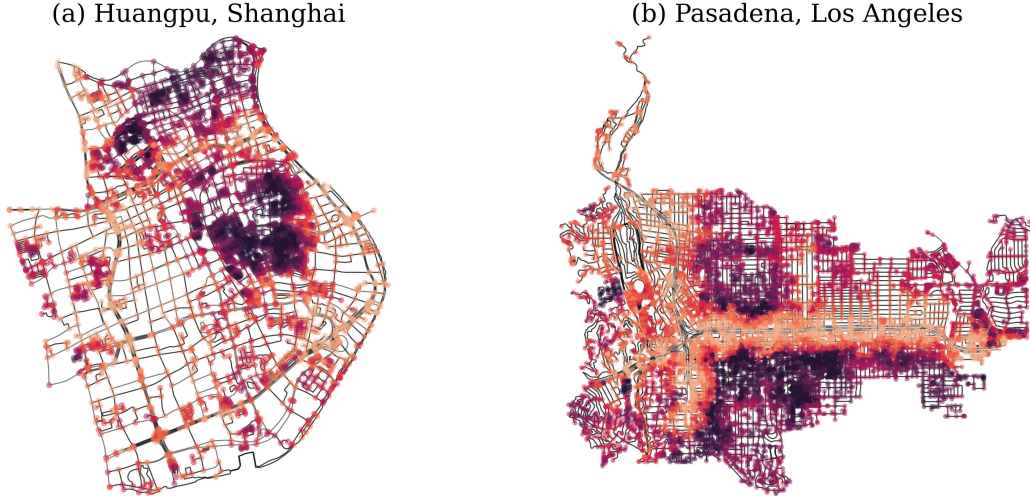


Figure 2: Visualizations of node eccentricity estimations on (a) Huangpu, Shanghai and (b) Pasadena, L.A., where **darker** colors indicate **smaller** eccentricity values, i.e., nodes that are easier to access.

ego-network centered at  $v$ , and compute an approximation,  $\hat{\varepsilon}(v)$ , based on this subgraph. Although this might seem like a computational limitation in principle, it actually allows us to know a priori that the long-range signal should be highly correlated with the 16th hop, as we later observe in Section 3. To design a classification task, we split the eccentricities for all nodes into 10 quantiles which we use as node labels. Note that, in contrast, LRGB uses the semantic context of an image after segmentation as labels and treats the synthetic super-pixels as graph nodes, whereas `City-Networks` is derived from real-world road networks and is therefore a more realistic and practical task that studies the accessibility of different neighbourhoods in a city. We refer readers to Appendix A.2 for more information on our feature construction and labeling approach.

**Visualizing labels and long-range dependency in `City-Networks`.** As shown in Equation (1), calculating node eccentricity  $\varepsilon(v)$  (or its approximation  $\hat{\varepsilon}(v)$ ) naturally requires information from distant-hop neighbors, and it carries a practical meaning which relates to the general accessibility of node  $v$  in the network. For instance, for locations in the city center, where the network is more interconnected, eccentricities tend to be lower than in rural areas with sparser road connections. To intuitively understand the node labels, we provide two visualizations of Huangpu, Shanghai, and Pasadena, Los Angeles in Figure 2. Interestingly, since we are using the approximation  $\hat{\varepsilon}(v)$  based on node  $v$ 's 16-hop neighborhood, nodes on major transportation routes such as freeways and highways will tend to have larger eccentricities than those in populated areas. This is because reaching a node's 16th-hop neighbors from a highway junction often requires traveling a much longer distance compared to road junctions in a downtown area. Based on Figure 2, it is also clear that a significant part of the graph topology is grid-like and possibly quasi-isometric to a lattice, as we will later discuss in Section 6. Note that the graph homophily scores, as shown in Table 1, will not be necessarily low in this case, since nodes with similar  $\hat{\varepsilon}$  tend to cluster together.

Large networks present a significant challenge for both GNNs and Graph Transformers since they must process features from a node's distant neighbors—such as their coordinates, land use, and surrounding road characteristics—to accurately determine the target node's eccentricity. In particular, this requirement creates a fundamental trade-off for GNNs: while increasing the number of layers helps propagate information from distant hops, it also leads to issues such as over-smoothing (Li et al., 2018; Nt & Maehara, 2019; Rusch et al., 2023), over-squashing (Alon & Yahav, 2021; Topping et al., 2022; Di Giovanni et al., 2023), and potential over-parameterization. Similarly, Graph Transformers, which rely on attention mechanisms with quadratic computational complexity, face scalability challenges when applied to our large-scale city networks with long diameters, making it more difficult to efficiently capture global structural information compared to learning on smaller graphs like those in LRGB.

### 3 Benchmarks: From Classical GNNs to Graph Transformers

In this section, we benchmark our dataset by comparing the empirical performance of classical GNNs and Graph Transformers under different experimental settings. We emphasize at the outset that the primary objective of our experiments is to demonstrate the presence of long-range dependencies in the proposed City-Networks with associated task, rather than maximizing each model’s performance with its optimal hyperparameters. Readers are referred to Appendix B for more training details and our experiment settings.

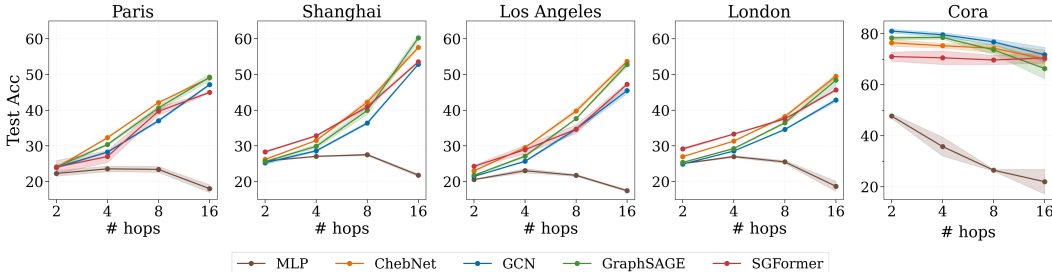


Figure 3: Results for setting number of layers  $L$  to match number of hops  $H \in [2, 4, 8, 16]$ .

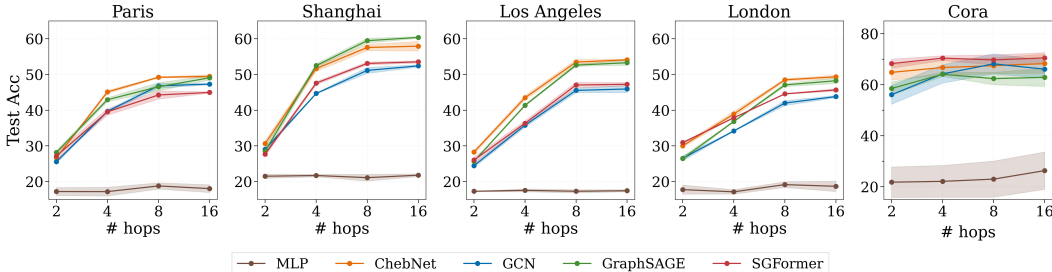


Figure 4: Results for fixing number of layers  $L = 16$  and setting numbers of hops  $H \in [2, 4, 8, 16]$ .

**Experimental setups.** We consider transductive node classification and split train/validation/test sets by 10%/10%/80% on all networks, where we fix the data split for benchmarking purposes, and adopt the average classification accuracy as our evaluation metric. For baselines, we consider both spectral and spatial GNNs: ChebNet (Defferrard et al., 2016), GCN (Kipf & Welling, 2017), and GraphSAGE (Hamilton et al., 2017); and a scalable Graph Transformer, SGFormer (Wu et al., 2023), which combines local message-passing and linear global attention. In addition, we also include an MLP without using graph information to reflect the importance of topology in our task. All the baselines are implemented with standard methods in PyTorch Geometric (PyG) (Fey & Lenssen, 2019) if available or otherwise based on their officially released codes. During training, all models are optimized for  $20k$  epochs using AdamW (Loshchilov & Hutter, 2019) with a learning rate of  $10^{-3}$  and a weight decay of  $10^{-5}$ . At the end of training, we select the epoch with the best validation performance and record its corresponding test accuracy. We then report the mean and standard deviation of the test accuracies across 5 runs.

**Scalable training with  $H$ -hop sampling.** Since the full-batch training is infeasible on our large-scale city networks, we adopt a standard mini-batching method (Hamilton et al., 2017) implemented by PyG-NeighborLoader, which first samples  $S$  seed nodes and grows an  $H$ -hop neighborhood for each seed node (i.e. an  $H$ -hop ego-network). At each iteration in the loader, these subgraphs will then be batched together and sent to the model to generate predictions on the seed nodes only. Importantly, this method implies that the model can only observe information from maximally  $H$  hops, which enables us to investigate the long-range dependency by controlling  $H$  and then comparing the model’s performance. Specifically, we test each baseline with different numbers of hops at  $H \in [2, 4, 8, 16]$  under two settings: (1) matching the number of layers  $L$  to  $H$ , and (2) fixing the number of layers to  $L = 16$  (i.e. freeze the model size) for different  $H$ . For experimental purposes, we employ a fixed hidden channel size of 32 in all baselines to maintain a comparable parameter size across models.

**Results.** The results for settings (1) and (2) are shown in Figure 3 and Figure 4, respectively. When matching  $L = H$  and gradually increasing the number of sampled hops  $H$ , we can observe a clear improvement in performance for all baselines on our four city networks, while on Cora, the baselines all suffer from over-smoothing, except for SGFormer<sup>4</sup>, whose performance remains relatively stable. This result suggests that incorporating information from more distant hops will improve both GNNs and Graph Transformers’ performance on City-Networks, but such gain is outweighed by over-smoothing issues on Cora due to the increasing number of GNN layers. On the other hand, one could argue that the observed performance gains may be attributed to the increasing model parameters as the number of layers  $L$  grows. To address this, we further investigate the scenario where  $L$  is fixed at 16 (i.e., keeping the model size constant) while gradually increasing  $H$ . Similar to the previous results, all baselines exhibit a consistent upward trend on our proposed dataset, whereas no clear pattern emerges on Cora (all baselines are subject to over-smoothing in this case). We interpret these results that long-range dependency is the primary factor that contributes to the improvement of baselines’ performance as  $H$  increases, and we proceed to introduce a quantitative measure of such dependency in the next section.

Table 2: Baseline results of the best testing accuracy on City-Networks.

Baseline	Paris	Shanghai	Los Angeles	London
MLP	23.6 ± 0.8	27.5 ± 0.3	23.1 ± 0.6	27.0 ± 0.3
ChebNet	49.5 ± 0.4	57.9 ± 1.4	54.1 ± 0.2	49.4 ± 0.4
GCN	47.3 ± 0.2	52.4 ± 0.3	45.9 ± 1.0	43.8 ± 0.3
GraphSAGE	49.1 ± 0.6	60.4 ± 0.3	53.3 ± 0.7	48.2 ± 0.8
SGFormer	45.0 ± 0.2	53.5 ± 0.3	47.2 ± 0.5	45.7 ± 0.3

For reference, we also summarize the best performance of the baselines on our City-Networks in Table 2, which, as expected, all occur at  $L = H = 16$ . We reiterate that, through the above analysis, our primary goal is to demonstrate the long-range dependencies in the data and task manifested in model performance. It is important to note that the reported results may not reflect the optimal performance of these baselines, which constitutes a limitation of this study and is further discussed in Appendix B.

## 4 Quantifying Long-Rangeness: A Measurement Based on Jacobians

In this section, we propose to quantify the long-range dependency of a task given a trained model by seeing how the *influence score*  $I(v, u)$  between node-pairs (Xu et al., 2018; Gasteiger et al., 2022) varies with distance, which measures the sensitivity of a GNN layer at node  $v$  to the input feature of node  $u$  using the Jacobian:

$$I(v, u) = \sum_i \sum_j \left| \frac{\partial \mathbf{H}_{vi}^{(L)}}{\partial \mathbf{X}_{uj}} \right|, \quad (2)$$

where  $\mathbf{H}_{vi}^{(L)}$  is the  $i^{\text{th}}$  entry of node  $v$ ’s embedding at layer  $L$ , and  $\mathbf{X}_{uj}$  is the  $j^{\text{th}}$  entry of the input feature vector for node  $u$ . Unless otherwise specified, we assume  $L$  refers to the last logit layer (pre-softmax inputs).

Based on the influence score, we define the *average total influence*  $\bar{T}_h$  at  $h^{\text{th}}$  hop as:

$$T_h(v) = I_{\text{sum}}(v, h) = \sum_{u: \rho(v, u)=h} I(v, u), \quad \bar{T}_h = \frac{1}{N} \sum_v I_{\text{sum}}(v, h), \quad (3)$$

where  $T_h(v) = I_{\text{sum}}(v, h)$  is the *total influence* from the  $h^{\text{th}}$ -hop neighbors of node  $v$ ,  $\rho(v, u)$  is the length of the shortest path between  $v$  and  $u$  (note that this is equivalent to the  $h$ -hop shell later discussed in Section 6.3), and  $N$  is the number of nodes in the network. Also, we would like to highlight that when  $h = 0$ ,  $T_0(v) = I(v, v)$  becomes the influence of the feature at node  $v$  on its output. The average total influence quantifies how much, on average, the features of nodes that are  $h$  hops away affect the output at the focal node. In other words, by summing the Jacobian-based

<sup>4</sup>We use the default split on Cora for all baselines rather than the random split from the SGFormer paper.

Table 3: The average size of the influence-weighted receptive field  $R$  on different datasets, where the underlying models are trained with  $L = H = 16$  from Section 3.

Model	Paris	Shanghai	L.A.	London	Cora	Citeseer	ogbn-arxiv
GCN	4.01	4.58	5.34	6.19	3.25	1.53	1.33
ChebNet	6.30	4.89	6.77	7.62	2.33	0.86	2.98
GraphSAGE	5.79	5.83	6.69	7.19	2.28	0.66	1.33
SGFormer	3.86	4.62	4.05	4.65	0.77	0.51	1.53

influence scores from all  $h$ -hop neighbors (or shells) and then averaging over all nodes, it provides an *expected measure of the cumulative effect that distant nodes have on each node as the focal node*.

Given Equation (3), we further define the average size  $R$  of the *influence-weighted receptive field* as:

$$R = \frac{1}{N} \sum_{v \in V} \frac{\sum_{h \geq 0}^H h \cdot T_h(v)}{\sum_{h \geq 0}^H T_h(v)}, \quad (4)$$

where  $H$  is the maximum number of hops to be considered. Intuitively, one can understand  $R$  as measuring *how far away the average unit of influence is*, where graphs with long-range dependencies are expected to have higher proportional influence between more distant nodes. We refer readers to Appendix C for a discussion on the computational cost of this measurement.

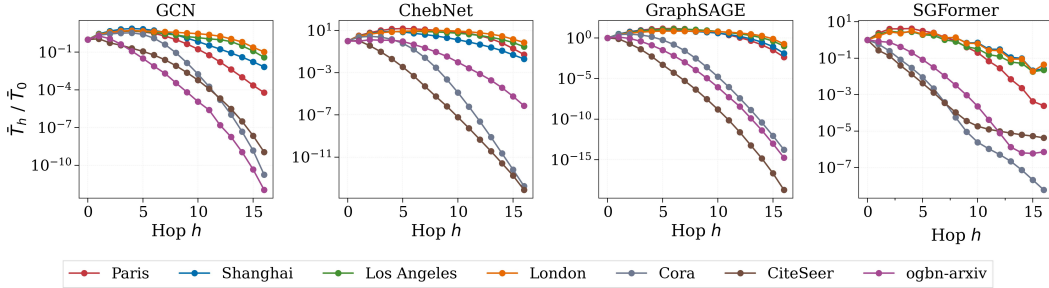


Figure 5: Normalized average total influence  $\bar{T}_h / \bar{T}_0$  averaged across nodes at different distances.

**Empirical results.** We validate  $R$  and  $\bar{T}_h$  on our datasets using four models from Section 3, each with 16 layers and trained using 16-hop neighborhood sampling (i.e.,  $H = L = 16$ ). To analyze long-range dependencies, we also train these models on Cora, Citeseer, and ogbn-arxiv under identical settings and compare their behavior in this setting to the patterns on City-Networks. The results in Table 3 show that  $R$  is consistently higher on our City-Networks compared to the citation networks across all models, which indicates a longer range of influence. To make  $\bar{T}_h$  more comparable across models and datasets, we normalize it to  $\bar{T}_h / \bar{T}_0$  and present the results in Figure 5. We can observe that for all models, there is a clearer and more rapid decay of influence at distant hops in all citation networks compared to city networks. We note that  $R$  and  $\bar{T}_h$  are model-dependent; however, results on these measures provide a consistent ordering between datasets: our city networks and their associated tasks require trained models to consider features from further hops compared to citation networks when generating predictions.

For the rest of this paper, we will first provide a theoretical justification of the proposed dataset by linking over-smoothing to algebraic connectivity and network diameter in Section 5, and then present the intuition behind the proposed long-range measurement in Section 6.

## 5 Theoretical Justification of Graph Topologies in City-Networks

In this section, we provide a *spectral understanding of over-smoothing* in GNNs. We emphasize that, rather than offering an in-depth theoretical analysis, our aim is to justify our dataset design choices by grounding them in theoretical foundations. The section is organized as follows. First, we review the concept of information loss in the limit of infinite GNN layers due to over-smoothing. We

show that over-smoothing effectively vanishes the original node features and makes representations collapse to a value that is only dependent on the graph topology. Next, we prove that the rate at which over-smoothing happens is controlled by the eigenvalues of the normalized adjacency operator in linear GCNs. Given that eigenvalues with larger absolute values slow down over-smoothing, we analyze how the magnitude of the eigenvalues relates to the graph topology of our datasets. In particular, we show that sparse graphs with large diameters promote bigger positive eigenvalues for the normalized adjacency operator and hence are less vulnerable to over-smoothing. Finally, we argue that less over-smoothing makes it possible for GNNs to build long-range representations in the case of our proposed dataset. All proofs are presented in Appendix D.1.

## 5.1 Preliminaries: A Spectral Perspective on Over-smoothing for Linear GCNs

We begin by analyzing over-smoothing through the lens of linearization, following the framework established in Wu et al. (2019) to build Simple Graph Convolutional Networks (SGCs). We select this model for our analysis because it is a linearized and more interpretable version of the widely adopted GCN model; in our empirical study in Section 3, we use the widely adopted classical GCN. Linear convolutions have also been used for theoretical analysis in other previous works such as Giovanni et al. (2022). Although GCNs are often regarded in recent literature as local neighborhood aggregators, they were originally derived from a spectral perspective. Thus, our analysis revisits the original conceptual foundation that motivated the model.

Let  $\mathcal{G} = (V, E)$  be an undirected graph with adjacency matrix  $\mathbf{A} \in \mathbb{R}^{N \times N}$  and degree matrix  $\mathbf{D} \in \mathbb{R}^{N \times N}$  ( $\mathbf{D}_{ii} = \sum_j \mathbf{A}_{ij}$ ), where  $N = |V|$  is the total number of nodes in the graph. The normalized (augmented) adjacency operator  $\tilde{\mathbf{S}}_{adj} \in \mathbb{R}^{N \times N}$  is defined as:

$$\tilde{\mathbf{S}}_{adj} = (\mathbf{I} + \mathbf{D})^{-\frac{1}{2}} (\mathbf{I} + \mathbf{A}) (\mathbf{I} + \mathbf{D})^{-\frac{1}{2}}, \quad (5)$$

where the original adjacency matrix and degree matrix have been augmented with self-loops leveraging the identity matrix  $\mathbf{I}$ . A Graph Convolutional Network (GCN) layer with input features  $\mathbf{X}^{(l)}$ , learnable weights  $\mathbf{W}^{(l)}$  for layer  $l$ , and non-linear pointwise activation function  $\sigma$  is defined as:

$$\mathbf{X}^{(l+1)} = \sigma \left( \tilde{\mathbf{S}}_{adj} \mathbf{X}^{(l)} \mathbf{W}^{(l)} \right). \quad (6)$$

As pointed out in Wu et al. (2019), under linearization (removal of non-linear activations), an  $L$ -layer Simple Graph Convolution (SGC) can be expressed as:

$$\mathbf{X}^{(L)} = (\tilde{\mathbf{S}}_{adj})^L \mathbf{X}^{(0)} \left( \prod_{l=0}^{L-1} \mathbf{W}^{(l)} \right), \quad (7)$$

where  $(\tilde{\mathbf{S}}_{adj})^L$  is the  $L$ -th power of the normalized adjacency operator. The result follows directly from iterative application of the linearized GCN operation.

Next, it is well known that the normalized adjacency operator  $\tilde{\mathbf{S}}_{adj}$  admits an eigendecomposition:

$$\tilde{\mathbf{S}}_{adj} = \tilde{\mathbf{U}} \mathbf{\Lambda} \tilde{\mathbf{U}}^T, \quad (8)$$

where  $\mathbf{\Lambda} = \text{diag}(\lambda_1, \dots, \lambda_N)$  with  $\lambda_1 < \dots < \lambda_N$  and  $\tilde{\mathbf{U}}$  contains the corresponding eigenvectors. And, for any positive integer  $k$ , the power iteration is as follows:

$$(\tilde{\mathbf{S}}_{adj})^k = \tilde{\mathbf{U}} \mathbf{\Lambda}^k \tilde{\mathbf{U}}^T, \quad (9)$$

where  $\mathbf{\Lambda}^k = \text{diag}(\lambda_1^k, \dots, \lambda_N^k)$ .

Wu et al. (2019) discuss the spectral properties of the normalized adjacency operator, which satisfies:  $\lambda_N = 1$ , and  $|\lambda_i| < 1$  for all  $i < N$ . Therefore, as the number of layers approaches infinity, the layer collapse phenomenon is well-documented in the literature:

$$\lim_{l \rightarrow \infty} (\tilde{\mathbf{S}}_{adj})^l = \tilde{\mathbf{u}}_N \tilde{\mathbf{u}}_N^T, \quad (10)$$

where  $\tilde{\mathbf{u}}_n$  is the eigenvector corresponding to  $\lambda_N$ . This is because as  $l \rightarrow \infty$ ,  $\lambda_i^l \rightarrow 0$  for all  $i < N$  since  $|\lambda_i| < 1$ . Meanwhile,  $\lambda_N^l = 1^l = 1$  for all  $l$ . Thus,

$$\lim_{l \rightarrow \infty} (\tilde{\mathbf{S}}_{adj})^l = \tilde{\mathbf{U}} \begin{pmatrix} 0 & & \\ & \ddots & \\ & & 1 \end{pmatrix} \tilde{\mathbf{U}}^T = \tilde{\mathbf{u}}_N \tilde{\mathbf{u}}_N^T. \quad (11)$$



This ultimately leads to information loss. In the limit as  $k \rightarrow \infty$ , the graph convolution operation collapses all node features to scalar multiples of  $\tilde{\mathbf{u}}_n$ , the entry of which at node  $v$  is  $\sqrt{1 + \text{degree}(v)}$ , resulting in complete loss of the original feature information. In other words, the learned representations suffer from *over-smoothing*.

## 5.2 Over-smoothing Rate as a Function of Algebraic Connectivity, Diameter, and Sparsity

Next, we provide intuition about the types of graph topologies that would mitigate the over-smoothing problem. In particular, sparse graphs—those lacking the small-world effect commonly found in citation networks—and graphs with large diameters tend to experience over-smoothing at a slower rate. We argue that this slower rate of over-smoothing implies a higher likelihood that GNNs can learn long-range dependencies during optimization. We show this intuition by bounding the eigenvalues of the normalized adjacency matrix using graph properties, then showing how these eigenvalues influence over-smoothing, and thus how controlling these graph properties can mitigate over-smoothing.

Recall that the normalized Laplacian matrix  $\mathbf{L}_{sym}$  of a graph is defined as:

$$\mathbf{L}_{sym} = \mathbf{I} - \mathbf{D}^{-\frac{1}{2}} \mathbf{A} \mathbf{D}^{-\frac{1}{2}} = \mathbf{I} - \mathbf{S}_{adj}, \quad (12)$$

which is intimately related to the normalized adjacency operator,  $\tilde{\mathbf{S}}_{adj}$ . Also, recall that the normalized algebraic connectivity  $\lambda_2(\mathbf{L}_{sym})$  is defined as the second smallest eigenvalue of  $\mathbf{L}_{sym}$ . For connected graphs like ours,  $\lambda_2(\mathbf{L}_{sym}) > 0$ . We first present the following lemma.

**Lemma 5.1** (Eigenvalue complementarity of normalized operators). For a connected graph, the eigenvalues  $\mathbf{S}_{adj}$  and  $\mathbf{L}_{sym}$  exhibit the following complementarity relationship:

$$\lambda_{N+1-i}(\mathbf{S}_{adj}) = 1 - \lambda_i(\mathbf{L}_{sym}) \quad (13)$$

for all  $i = 1, \dots, N$ , where  $N$  is the number of nodes in the graph, and eigenvalues (for both operators) are indexed such that  $\lambda_1 \leq \lambda_2 \leq \dots \leq \lambda_N$ .

This complementarity implies that when the normalized algebraic connectivity  $\lambda_2(\mathbf{L}_{sym})$  is small, the second largest positive eigenvalue of  $\mathbf{S}_{adj}$  must be close to 1. However, in our context, we are interested in the algebraic connectivity of the normalized graph Laplacian that would correspond to the normalized adjacency operator,  $\tilde{\mathbf{S}}_{adj}$ , introduced in Equation (5), instead of that of  $\mathbf{S}_{adj}$ . Thus, we extend (Wu et al., 2019, Theorem 1) to cover the normalized algebraic connectivity:

**Proposition 5.2** (Self-loops decrease algebraic connectivity of the original graph). Assume a connected graph  $\mathcal{G}$ . For all  $\gamma > 0$ ,

$$\lambda_{N-1}(\mathbf{S}_{adj}) = \lambda_{N-1} \left( \mathbf{D}^{-\frac{1}{2}} \mathbf{A} \mathbf{D}^{-\frac{1}{2}} \right) < \lambda_{N-1} \left( (\gamma \mathbf{I} + \mathbf{D})^{-\frac{1}{2}} (\gamma \mathbf{I} + \mathbf{A}) (\gamma \mathbf{I} + \mathbf{D})^{-\frac{1}{2}} \right). \quad (14)$$

That is, the second largest positive eigenvalue of the normalized adjacency operator of a graph with self-loops is larger than that of the same graph without self-loops, since adding self-loops “sparsifies” the original graph and reduces its algebraic connectivity. This allows us, via Lemma 5.1, to relate the second largest positive eigenvalue of  $\tilde{\mathbf{S}}_{adj}$  to the topology of graphs in the proposed dataset, using bounds similar to those presented in (Chung, 1997, Lemma 1.14).

**Theorem 5.3** (Bound on second largest positive eigenvalue of the normalized adjacency operator). Let  $d_{max}$  be the maximum degree of a vertex in  $\mathcal{G}$ , and  $diam(\mathcal{G})$  the diameter of  $\mathcal{G}$ , which must be  $diam(\mathcal{G}) \geq 4$ . Then

$$\lambda_{N-1}(\tilde{\mathbf{S}}_{adj}) > \frac{2\sqrt{d_{max}-1}}{d_{max}} - \frac{2}{diam(\mathcal{G})} \left( 1 + \frac{2\sqrt{d_{max}-1}}{d_{max}} \right). \quad (15)$$

From Table 4, we see that the lower bound in Equation (15) is generally higher for our datasets; this is because the bound is decreasing in  $d_{max}$  and increasing in  $diam(\mathcal{G})$ , showing graphs with large diameter and low maximum degree will be more resilient to over-smoothing. We provide the rationale as follows.

Table 4: The lower bound for  $\lambda_{N-1}(\tilde{\mathcal{S}}_{adj})$  on different datasets.

Dataset	City-Network (ours)				LRGB		Planetoid		OGB
	Paris	Shanghai	L.A.	London	PascalVOC	COCO	Cora	CiteSeer	ogbn-arxiv
Bound	0.4741	0.6344	0.6095	0.5921	0.4857	0.4815	0.0324	0.1143	-0.0640

The second largest eigenvalue of  $\tilde{\mathcal{S}}_{adj}$  in terms of magnitude is either  $\lambda_{N-1}$  or  $\lambda_1$ . We now explicitly consider the case when it is  $\lambda_{N-1}$ . As  $\lambda_{N-1}$  approaches 1, the rate of convergence to the limiting state  $\tilde{\mathbf{u}}_N \tilde{\mathbf{u}}_N^T$  decreases exponentially with the number of layers. For any layer  $l$ , the difference from the limiting state can be expressed as:

$$\|(\mathbf{I} - \tilde{\mathbf{u}}_N \tilde{\mathbf{u}}_N^T)(\tilde{\mathcal{S}}_{adj})^l\| = \|\tilde{\mathbf{U}} \text{diag}(\lambda_1^l, \dots, \lambda_{N-1}^l, 0) \tilde{\mathbf{U}}^T\| = \lambda_{N-1}^l \quad (16)$$

where  $\|\cdot\|$  denotes the spectral norm and the last equality follows from that the spectral norm of a diagonal matrix being equal to the largest absolute value of its diagonal entries. Thus, when  $\lambda_{N-1}$  is close to 1, more layers are required to achieve the same level of convergence to the limiting state. Since  $\lambda_{N-1} < 1$ , taking powers of  $\lambda_{N-1}$  will eventually converge to zero, but the rate of this convergence slows dramatically as  $\lambda_{N-1}$  approaches 1. Hence, because graphs with a large diameter and low maximum degree have a lower algebraic connectivity due to reduced inter-component connectivity, GNNs operating on such graphs will be less susceptible to over-smoothing when processing node features.

We have focused on the case where the second largest eigenvalue by magnitude of  $\tilde{\mathcal{S}}_{adj}$  is  $\lambda_{N-1}$ . The special case where it is instead  $\lambda_1$  (which, in this case, must be negative) gives a different regime, where it is possible for graphs with smaller diameters to exhibit less over-smoothing than those with larger diameters. Consider, for example, a bipartite graph where over-smoothing occurs independently on each side of the partition, resulting in two distinct values depending on which partition the node is in, rather than convergence to a multiple of  $\tilde{\mathbf{u}}_N$ , where the node feature value would only depend on the degree.

Nevertheless, our analysis demonstrates that large diameters and sparse connectivity generally mitigate over-smoothing. This insight motivates our proposal of benchmark datasets with significantly larger diameters than those currently used in the literature, refer back to Table 1. The underlying hypothesis is that reduced over-smoothing in high-diameter, sparse networks enables the possibility of GNNs learning representations that capture long-range dependencies when necessary.

## 6 Theoretical Justification of Jacobian-Based Measurement

Lastly, in this section, we provide the intuition behind the proposed measurement for quantifying long-rangeness in Section 4. In particular, we discuss potential limiting cases and provide a theoretical understanding of *influence score dilution* for lattice and grid-like graphs, which supports the construction of the proposed measurement. The proofs for all lemmata, propositions, and theorems can be found in Appendix D.2.

### 6.1 Intuition behind Jacobian-based Influence Score

The Jacobian has been used in analysis of node interactions in GNNs in multiple previous works (Xu et al., 2018; Gasteiger et al., 2022; Di Giovanni et al., 2023). For example, it is used in Di Giovanni et al. (2023, Theorem 4.1) to show when over-squashing happens in long-range interactions, and to show how vanishing gradients occur in very deep GNNs. Influence specifically has been used to compute a natural measure of interactions between two nodes (Xu et al., 2018). We accordingly use aggregated influence, Equation (3), to gauge how nodes at a distance  $h$  affect the output of the GNN at a focal node, thus quantifying *long-rangeness*. By the definition of partial derivatives, we can understand the Jacobian as follows:

$$\frac{\partial \mathbf{H}_{vi}^{(\ell)}(\mathbf{X})}{\partial \mathbf{X}_{uj}} = \lim_{\delta \rightarrow 0} \frac{\mathbf{H}_{vi}^{(\ell)}(\mathbf{X} + \delta \mathbf{e}_{uj}) - \mathbf{H}_{vi}^{(\ell)}(\mathbf{X})}{\delta}, \quad (17)$$

where  $\mathbf{X}$  is the original (unperturbed) input feature matrix, and  $\delta \mathbf{e}_{uj}$  is an infinitesimal perturbation in the  $j^{\text{th}}$  component of the feature vector at node  $u$  (a standard basis vector in the feature space of

the node). This means the more positive the Jacobian entry is, the more a positive perturbation of the features at node  $u$  and component  $j$  will increase the logits at node  $v$  and component  $i$  at the final layer. In other words, the Jacobian entry being positive or negative means that the logits are pushed up or down. Given that, after applying the softmax function, the probabilities at a given data point increase monotonically with the logits at that point<sup>5</sup>, we can consider both positive and negative influences as actual influence and only need to focus on the absolute value (i.e., sensitivity rather than direction).

## 6.2 Potential Limitations: Output Cancellation

However, it is possible to find counterexamples in which measuring the absolute Jacobian sensitivity could be insufficient or even misleading: if a positive and negative influence always cancel each other out. We find such a situation can happen in unregularised linear models with heavy collinearity of features (Hastie et al., 2009, p.63) – indeed, this is presented as one of the motivations of ridge regression. To better understand this, we give a simple model of such cancellation:

**Proposition 6.1** (Absolute Jacobian sensitivity may over-estimate influence). There exists a model  $k$  with zero net derivative (i.e.,  $k'(\mathbf{X}) = 0 \ \forall \mathbf{X}$ ) for which the sum of the absolute values of individual Jacobian contributions is nonzero.

The proof relies on constructing a toy function with two branches that counteract each other exactly for any input, see Appendix D.2. The nonzero value in the proposition suggests a strong sensitivity to perturbations in  $\mathbf{X}$  even though the net change in the output  $k(\mathbf{X})$  is zero. Thus, this counterexample demonstrates that measuring influence solely via the absolute values of the Jacobian entries can be misleading when opposing contributions cancel in the final output. Although this is a valid concern, we next show that for Message Passing Neural Networks (MPNNs), at least at initialization, such cancellation does not happen.

**Definition 6.2** (Message-Passing Neural Network layer). For a MPNN layer  $l$ , the node feature update for  $v$  is given by:  $\mathbf{X}_v^{(l+1)} = \phi\left(\mathbf{X}_v^{(l)}, \bigoplus_{u \in \mathcal{N}(v)} \psi\left(\mathbf{X}_v^{(l)}, \mathbf{X}_u^{(l)}\right)\right)$ , where  $\psi$  is a message function, responsible for computing interactions between neighboring nodes,  $\bigoplus$  is a permutation-invariant aggregation function, such as summation, mean, or max,  $\phi$  is an update function that integrates aggregated information into the node representation.

**Theorem 6.3** (Measure-zero of exact cancellation at MPNN initialization). Consider an MPNN where the functions  $\psi$  and  $\phi$  are parameterized by  $\theta$  and differentiable, typically modeled as MultiLayer Perceptrons (MLPs). Suppose the parameters  $\theta$  are drawn from a probability distribution that is absolutely continuous with respect to the Lebesgue measure. Then, the set of parameter configurations for which exact cancellation of Jacobian contributions occurs has Lebesgue measure zero.

## 6.3 Justification of Proposed Measurement and the Mean Influence Score Dilution Problem

Finally, we justify the proposed measurement for analyzing long-range interactions in GNNs, particularly by comparing the mean and the sum of influence scores of neighboring nodes as candidates to represent the *total influence score* for a focal node  $v$ ,  $T_h(v)$ . Recall that  $T_h(v) = I_{\text{sum}}(v, h) = \sum_{u: \rho(v,u)=h} I(v, u)$  as in Equation (3). We first revise important notions such as that of the standard lattice in Euclidean space,  $h$ -hop shells, and quasi-isometric graphs, and then provide a mathematical analysis of influence score dilution. This helps justify the construction of  $T_h(v)$  as a sum rather than a mean operator, which is key to the computation of the *average total influence* in Equation (3) and the *influence-weighted receptive field* in Equation (4).

**Definition 6.4** (Standard lattice in  $\mathbb{R}^D$ ). The *standard lattice* in  $\mathbb{R}^D$ , denoted by  $\mathbb{Z}^D$ , is the set of all integer-coordinate points in  $\mathbb{R}^D$ :  $\mathbb{Z}^D = \{(z_1, z_2, \dots, z_D) \mid z_i \in \mathbb{Z} \text{ for all } i = 1, \dots, D\}$ . Equivalently,  $\mathbb{Z}^D$  consists of all points that can be written as integer linear combinations of the standard basis vectors:  $\mathbb{Z}^D = \left\{ \sum_{i=1}^D z_i \mathbf{e}_i \mid z_i \in \mathbb{Z} \right\}$ , where  $\{\mathbf{e}_1, \mathbf{e}_2, \dots, \mathbf{e}_D\}$  is the standard basis for  $\mathbb{R}^D$ , meaning each  $\mathbf{e}_i$  is a unit vector with a 1 in the  $i$ -th position and 0 elsewhere. This lattice forms a grid-like structure in  $\mathbb{R}^D$  with each point having exactly  $2D$  one-hop (adjacent lattice) neighbors. For a planar graph  $D = 2$ , hence, each node has a total of 4 neighbors.

<sup>5</sup>It is well-known that for a vector of logits the softmax probabilities are monotonically increasing with respect to their corresponding logits. Also see Appendix D.2 for a proof.

**Definition 6.5** (*h-hop shells*). Let  $\mathcal{G} = (V, E)$  be a graph with shortest-path distance  $\rho : V \times V \rightarrow \mathbb{N}$ . The *h-hop shell* (or *h-hop neighborhood*) of a node  $v \in V$  is defined as  $\mathcal{N}_h(v) = \{u \in V : \rho(v, u) = h\}$ . That is,  $\mathcal{N}_h(v)$  consists of all nodes that are exactly  $h$  hops away from  $v$ .

**Definition 6.6** (*Quasi-isometric graphs*). Let  $\mathcal{G}_1 = (V_1, E_1)$  and  $\mathcal{G}_2 = (V_2, E_2)$  be two graphs equipped with shortest-path distance functions  $\rho_1 : V_1 \times V_1 \rightarrow \mathbb{R}_{\geq 0}$  and  $\rho_2 : V_2 \times V_2 \rightarrow \mathbb{R}_{\geq 0}$ , respectively (in our case distances are in  $\mathbb{N}$ ). We say that  $\mathcal{G}_1$  and  $\mathcal{G}_2$  are *quasi-isometric* if there exist constants  $\lambda \geq 1$ ,  $\mathfrak{C} \geq 0$ , and  $\mathfrak{D} \geq 0$ , and a function  $f : V_1 \rightarrow V_2$  such that for all  $u, v \in V_1$ :  $\frac{1}{\lambda}\rho_1(u, v) - \mathfrak{C} \leq \rho_2(f(u), f(v)) \leq \lambda\rho_1(u, v) + \mathfrak{C}$ . Every node in  $V_2$  is within distance  $\mathfrak{D}$  of some  $f(u)$ , i.e.,  $\forall v \in V_2, \exists u \in V_1$  such that  $\rho_2(v, f(u)) \leq \mathfrak{D}$ .

**Lemma 6.7** (*Growth of h-hop shells in grid-like graphs*). Let  $\mathcal{G} = (V, E)$  be a graph that is *grid-like* in  $D$  dimensions (e.g., let us presume the graphs in the proposed dataset are a subgraph of  $\mathbb{Z}^D$  or quasi-isometric to it, which seems reasonable given Figure 2) and assume the node degrees are uniformly bounded. Then, there exist positive constants  $\mathfrak{C}_1$  and  $\mathfrak{C}_2$  (depending on  $D$  and the local geometry of  $\mathcal{G}$ ) and an integer  $h_0$  such that for all  $h \geq h_0$ ,

$$\mathfrak{C}_1 h^{D-1} \leq |\mathcal{N}_h(v)| \leq \mathfrak{C}_2 h^{D-1}. \quad (18)$$

Given the definitions above, and after having quantified the growth of the  $h$ -hop shell, one can prove the following theorem, which motivates our aggregation choice.

**Theorem 6.8** (*Dilution of mean aggregated influence in grid-like graphs*). Suppose that for a fixed  $v$  and for each  $h \geq h_0$  there exists a distinguished node  $u^* \in \mathcal{N}_h(v)$  with a strong influence on  $v$ , quantified by  $I(v, u^*) = I^* > 0$ , while for all other nodes  $u \in \mathcal{N}_h(v) \setminus \{u^*\}$  the influence  $I(v, u)$  is negligible (or zero). Define  $I_{\text{sum}}(v, h) = \sum_{u \in \mathcal{N}_h(v)} I(v, u) = \sum_{u: \rho(v, u) = h} I(v, u)$  and  $I_{\text{mean}}(v, h) = \frac{1}{|\mathcal{N}_h(v)|} \sum_{u \in \mathcal{N}_h(v)} I(v, u)$ . Then,  $I_{\text{sum}}(v, h) \geq I^*$ , and  $I_{\text{mean}}(v, h) \leq \frac{I^*}{\mathfrak{C}_1 h^{D-1}}$ . Hence, as  $h \rightarrow \infty$ , we have  $I_{\text{mean}}(v, h) \rightarrow 0$ , while  $I_{\text{sum}}(v, h)$  remains bounded below by  $I^*$ . This also holds for planar graphs, where  $D = 2$ .

**Corollary 6.9** (*Dilution for a planar grid-like graph*). The dilution of the mean aggregated influence for a planar grid-like graph (like our city networks) is proportional to  $\frac{1}{h}$ .

**Corollary 6.10** (*Faster dilution over aggregated h-hop neighborhoods*). Let  $\mathcal{G}$  be a grid-like graph in  $D$  dimensions, and define the aggregated  $h$ -hop neighborhood (or ball) of a node  $v$  as  $B_h(v) = \bigcup_{i=1}^h \mathcal{N}_i(v)$ . As before, suppose that within  $B_h(v)$  there exists a unique node  $u^*$  with influence  $I(u^*, v) = I^* > 0$  and that for all other nodes  $u \in B_h(v) \setminus \{u^*\}$ , the influence is negligible. Then, the mean aggregated influence is diluted at a rate proportional to  $1/h^D$ . In particular, for a planar graph ( $D = 2$ ), the dilution occurs at a rate proportional to  $1/h^2$ .

Hence, this analysis formally justifies the choice in Equation (3), which considers the aggregate influence of neighboring nodes  $T_h(v) = I_{\text{sum}}$  as a more reliable measure than the mean  $I_{\text{mean}}$ , which is susceptible to dilution, particularly in the case of distant neighbors. Finally, note the following:

**Corollary 6.11** (*The dilution problem does not affect the average total influence*). Let  $T_h(v) = I_{\text{sum}}(v, h)$  be the total influence from the  $h$ -hop neighborhood  $\mathcal{N}_h(v)$  of node  $v$ , and let  $\bar{T}_h = \frac{1}{|V|} \sum_{v \in V} T_h(v)$  be the average total influence over all nodes in  $V$ . Suppose that for every  $v$  and every  $h$  there exists at least one distinguished node  $u^* \in \mathcal{N}_h(v)$  satisfying  $I(v, u^*) \geq I^* > 0$ . Then,  $\bar{T}_h \geq I^*, \forall h$ .

## 7 Conclusion

The main objective of our work is to provide better tools to help quantify long-range interactions in GNNs. Previous benchmarks, such as the LRGB (Dwivedi et al., 2023), are introduced in the context of small graph inductive learning, using solely the performance gap between classical GNNs and Graph Transformers to support the presence of long-range signals. In this work, we introduce a new large graph dataset based on city road networks, featuring long-range dependencies for transductive learning, and propose a principled measurement to quantify such dependencies. We also provide theoretical justification of both the proposed dataset and measurement, focusing on over-smoothing and influence score dilution. Beyond benchmarking purposes, our work also holds potential for a broader impact, informing applications in urban planning and transportation by providing tools to analyze and understand accessibility and influence within city road networks.

## References

- Alon, U. and Yahav, E. On the bottleneck of graph neural networks and its practical implications. In *International Conference on Learning Representations*, 2021.
- Boeing, G. Modeling and analyzing urban networks and amenities with osmnx. *Working paper*, 2024. URL <https://geoffboeing.com/publications/osmnx-paper/>.
- Borde, H. S. d. O. Elucidating graph neural networks, transformers, and graph transformers, 02 2024.
- Chung, F. R. *Spectral graph theory*, volume 92. American Mathematical Soc., 1997.
- Defferrard, M., Bresson, X., and Vandergheynst, P. Convolutional neural networks on graphs with fast localized spectral filtering. *Advances in neural information processing systems*, 29, 2016.
- Di Giovanni, F., Giusti, L., Barbero, F., Luise, G., Lio, P., and Bronstein, M. M. On over-squashing in message passing neural networks: The impact of width, depth, and topology. In *International Conference on Machine Learning*, pp. 7865–7885. PMLR, 2023.
- Dijkstra, E. A note on two problems in connexion with graphs. *Numerische Mathematik*, 1:269–271, 1959.
- Dwivedi, V. P., Rampásek, L., Galkin, M., Parviz, A., Wolf, G., Luu, A. T., and Beaini, D. Long range graph benchmark, 2023. URL <https://arxiv.org/abs/2206.08164>.
- Fey, M. and Lenssen, J. E. Fast graph representation learning with pytorch geometric. *arXiv preprint arXiv:1903.02428*, 2019.
- Floyd, R. W. Algorithm 97: Shortest path. *Commun. ACM*, 5(6):345, 1962. ISSN 0001-0782. doi: 10.1145/367766.368168.
- Gasteiger, J., Qian, C., and Günnemann, S. Influence-based mini-batching for graph neural networks. In *Learning on Graphs Conference*, pp. 9–1. PMLR, 2022.
- Giovanni, F. D., Rowbottom, J., Chamberlain, B. P., Markovich, T., and Bronstein, M. M. Understanding convolution on graphs via energies. *Trans. Mach. Learn. Res.*, 2023, 2022. URL <https://api.semanticscholar.org/CorpusID:258987606>.
- Hagberg, A., Swart, P. J., and Schult, D. A. Exploring network structure, dynamics, and function using networkx. Technical report, Los Alamos National Laboratory (LANL), Los Alamos, NM (United States), 2008.
- Haklay, M. and Weber, P. Openstreetmap: User-generated street maps. *IEEE Pervasive computing*, 7(4):12–18, 2008.
- Hamilton, W. L., Ying, R., and Leskovec, J. Inductive representation learning on large graphs. In *Proceedings of the 31st International Conference on Neural Information Processing Systems*, pp. 1025–1035, 2017.
- Hastie, T., Tibshirani, R., and Friedman, J. *The Elements of Statistical Learning*. Springer New York, 2009. ISBN 9780387848587. doi: 10.1007/978-0-387-84858-7. URL <http://dx.doi.org/10.1007/978-0-387-84858-7>.
- Hu, W., Fey, M., Zitnik, M., Dong, Y., Ren, H., Liu, B., Catasta, M., and Leskovec, J. Open graph benchmark: datasets for machine learning on graphs. In *Proceedings of the 34th International Conference on Neural Information Processing Systems*, pp. 22118–22133, 2020.
- Kipf, T. N. and Welling, M. Semi-supervised classification with graph convolutional networks. In *International Conference on Learning Representations*, 2017.
- Li, Q., Han, Z., and Wu, X.-M. Deeper insights into graph convolutional networks for semi-supervised learning. In *Proceedings of the AAAI conference on artificial intelligence*, volume 32, 2018.
- Loshchilov, I. and Hutter, F. Decoupled weight decay regularization. In *International Conference on Learning Representations*, 2019.

- Newman, M. *Networks*. Oxford university press, 2018.
- Nt, H. and Maehara, T. Revisiting graph neural networks: All we have is low-pass filters. *arXiv preprint arXiv:1905.09550*, 2019.
- Pei, H., Wei, B., Chang, K. C. C., Lei, Y., and Yang, B. Geom-gcn: Geometric graph convolutional networks. In *8th International Conference on Learning Representations, ICLR 2020*, 2020.
- Rusch, T. K., Bronstein, M. M., and Mishra, S. A survey on oversmoothing in graph neural networks. *arXiv preprint arXiv:2303.10993*, 2023.
- Scarselli, F., Gori, M., Tsoi, A. C., Hagenbuchner, M., and Monfardini, G. The graph neural network model. *IEEE Transactions on Neural Networks*, 20(1):61–80, 2009. doi: 10.1109/TNN.2008.2005605.
- Topping, J., Giovanni, F. D., Chamberlain, B. P., Dong, X., and Bronstein, M. M. Understanding over-squashing and bottlenecks on graphs via curvature. In *International Conference on Learning Representations, 2022*.
- Tönshoff, J., Ritzert, M., Rosenbluth, E., and Grohe, M. Where did the gap go? reassessing the long-range graph benchmark, 2023. URL <https://arxiv.org/abs/2309.00367>.
- Watts, D. J. and Strogatz, S. H. Collective dynamics of ‘small-world’ networks. *Nature*, 393(6684): 440–442, 1998. ISSN 1476-4687. doi: 10.1038/30918. URL <https://doi.org/10.1038/30918>.
- Wu, F., Souza, A., Zhang, T., Fifty, C., Yu, T., and Weinberger, K. Simplifying graph convolutional networks. In Chaudhuri, K. and Salakhutdinov, R. (eds.), *Proceedings of the 36th International Conference on Machine Learning*, volume 97 of *Proceedings of Machine Learning Research*, pp. 6861–6871. PMLR, 09–15 Jun 2019. URL <https://proceedings.mlr.press/v97/wu19e.html>.
- Wu, Q., Zhao, W., Yang, C., Zhang, H., Nie, F., Jiang, H., Bian, Y., and Yan, J. Simplifying and empowering transformers for large-graph representations. In *Advances in neural information processing systems*, 2023.
- Xu, K., Li, C., Tian, Y., Sonobe, T., Kawarabayashi, K.-i., and Jegelka, S. Representation learning on graphs with jumping knowledge networks. In *International conference on machine learning*, pp. 5453–5462. PMLR, 2018.
- Yang, Z., Cohen, W., and Salakhutdinov, R. Revisiting semi-supervised learning with graph embeddings. In *International conference on machine learning*, pp. 40–48. PMLR, 2016a.
- Yang, Z., Cohen, W. W., and Salakhutdinov, R. Revisiting semi-supervised learning with graph embeddings. In *Proceedings of the 33rd International Conference on International Conference on Machine Learning - Volume 48, ICML’16*, pp. 40–48. JMLR.org, 2016b.

## A Dataset Details

### A.1 Network Statistics

In this section, we explain the statistics used in Table 1 that characterize our dataset and discuss the estimation approach used when direct computation is impractical. We consider undirected graphs,  $\mathcal{G} = (V, E)$  with  $N = |V|$  nodes and  $|E|$  edges, where each node  $v$  is associated with a feature vector  $\mathbf{X}_v \in R^D$  and a label  $y_v \in \mathcal{Y}$  from a finite class set.

**Node degree.** The degree  $\deg(v)$  of a node  $v$  represents the number of edges adjacent to it. To characterize the distribution of node degree in a network, we consider its mean  $\mu_k$  and standard deviation  $\sigma_k$ :

$$\mu_k = \frac{1}{N} \sum_{v \in V} \deg(v), \quad \sigma_k = \sqrt{\frac{1}{N} \sum_{v \in V} (\deg(v) - \mu_k)^2}. \quad (19)$$

Importantly, networks of different topologies will have different degree distributions. For example, social networks often exhibit a power-law property, where a few nodes have high degrees while most nodes have relatively low degrees. As a result, their degree distribution tends to follow a scale-free pattern with a high degree variance  $\sigma_k^2$ . In contrast, grid-like networks, such as city networks and super-pixel graphs, have a structured layout of connections, leading to a more uniform degree distribution with lower variance.

**Clustering coefficient.** The clustering coefficient  $C_v$  measures the tendency of a node  $v \in V$  to form a tightly connected group based on triangles, and its average  $\bar{C}$  measures the overall level of clustering:

$$C_v = \frac{2T_v}{\deg(v)(\deg(v) - 1)}, \quad \bar{C} = \frac{1}{N} \sum_{v \in V} C_v, \quad (20)$$

where  $T_v$  is the number of triangles that include node  $v \in V$ . Alternatively, *transitivity* offers a global measure of clustering with the following expressions:

$$Transitivity = \frac{3 \times \text{number of triangles}}{\text{number of connected triples}}. \quad (21)$$

Intuitively, social networks tend to have a high *average clustering coefficient* and *transitivity* due to their community structure with highly connected hubs and frequent triadic closures. On the other hand, our city networks exhibit a low clustering coefficient and transitivity, as their structured and sparse connectivity (e.g., forming lattices) reduces the prevalence of triangles. Note that LRGB, although being “grid-like”, shows an even higher  $\bar{C}$  and transitivity than social networks. This is because its networks contain many triangles, as it uses semantic super-pixels as nodes with pixel borders being the edges.

**Diameter** The diameter  $D$  of a network is the longest shortest path between any two nodes:

$$D = \max_{u, v \in V} \rho(u, v), \quad (22)$$

where  $\rho(u, v)$  is the shortest path length from node  $u$  to node  $v$ . Note that in this case the distance is unweighted for a more direct comparison with other datasets. It represents the maximum communication delay in the network and varies significantly across different network structures. In social networks, the presence of hubs greatly reduces the average shortest path length, leading to a small-world effect with a relatively small diameter. In contrast, grid-like networks lack hubs, and their regular structure causes the diameter to increase more rapidly as the network size grows.

Since the exact calculation of  $D$  has a computational complexity  $\mathcal{O}(N^2 \log(N))$ , we use the following approach to estimate the approximate diameter  $\hat{D}$  of our city networks. For all nodes in a given city, we select the ones with the maximum and minimum latitude and longitude, respectively:  $coord(v_1) = (\cdot, lat_{max})$ ,  $coord(v_2) = (\cdot, lat_{min})$ ,  $coord(v_3) = (long_{max}, \cdot)$ , and  $coord(v_4) = (long_{min}, \cdot)$ . Based on these, we compute the shortest path between  $(v_1, v_2)$  and  $(v_3, v_4)$ , and take their maximum as our final diameter estimate, that is,  $\hat{D} = \max(d(v_1, v_2), d(v_3, v_4))$ . Note that the exact diameter  $D$  will always be larger than our estimation  $\hat{D}$ .

**Homophily.** The node homophily score (Pei et al., 2020) quantifies the tendency of nodes with the same label to be connected:

$$Homo = \frac{1}{N} \sum_{v \in V} \frac{|\{u \in \mathcal{N}(v) \mid y_u = y_v\}|}{|\mathcal{N}(v)|}, \quad (23)$$

where  $\mathcal{N}(v)$  is the set of neighbors of node  $v$ , and  $y_v$  represents the label of node  $v$ . A higher homophily indicates a stronger preference for connections between nodes of the same class, which can significantly impact the performance of GNN models.

## A.2 Feature and Label Construction

This section provides additional details of the features and labels of our City-Networks.

**Node and edge features.** Based on the raw city map queries, we obtained the following features on junctions and road segments:

- Three numerical features for the road junctions (nodes):
  - *latitude*: the latitude of the current road junction.
  - *longitude*: the longitude of the current road junction.
  - *street count*: the number of connected roads in both directions.
- One categorical features for the road junctions (nodes):
  - *land use*: the type of land use at the current coordinate: *residential, industrial, forest, farmland, commercial, railway*, etc.
- Two numerical features for road segments (edges):
  - *road length*: the length of the road in meters.
  - *speed limit*: the speed limit on the current road in km/h.
- Two binary features for road segments (edges):
  - *one-way*: if the current road can only be used in one direction by vehicles.
  - *reversed*: if the current road alternates between different directions during rush hours in the morning and evening, which is also sometimes called "tidal flow".
- Two categorical features for road segments (edges):
  - *lanes*: number of lanes in the current road, which takes either numerical values (e.g. 1, 2, 3, ...), or a list of numerical values (e.g. [1, 2], [2, 3], [4, 5], ...) when the current road has different number of lanes at different segments. We treat this feature as a categorical variable during modeling.
  - *road type*: the type of the current road, with possible values being: *service, residential, footway, primary, secondary, tertiary*, etc.

Since the categorical features *land use*, *lanes*, and *road type* contain many categories of only a few data points and varies across different networks, we only take the top 8 categories with most entries for each categorical feature, and treat the rest as a single category - *other*. Based on our observations, we can cover more than 90% of the network with the top 8 categories in all cases. This strategy leads to 12 node features and 25 edge features after one-hot encoding, that is, a total of 37 features after transferring edge features to their adjacent nodes by neighborhood aggregation. Finally, we transform the graph into an undirected one by merging all edges between each pair of nodes into a single edge, where the edge features are averaged using to\_undirected(reduce="mean") from PyG.

**Node labels based on eccentricity estimation.** As mentioned in Section 2, we use a 16-hop ego-network to estimate the eccentricity of each node. Specifically, after obtaining the neighborhood  $\mathcal{N}_{16}(v)$  within 16 hops of node  $v$ , we compute the shortest path from node  $v$  to all nodes within this neighborhood, and take the maximum as the estimated eccentricity  $\hat{\varepsilon}(v)$ :

$$\hat{\varepsilon}(v) = \max_{u \in \mathcal{N}_{16}(v)} \rho_w(v, u), \quad \rho_w(v, u) = \min_{\pi \in P(v, u)} \sum_{e \in \pi} w(e), \quad (24)$$



where  $\rho_w(v, u)$  is the weighted shortest path distance from node  $v$  to node  $u$ ,  $P(v, u)$  denotes the set of all possible paths from node  $v$  to node  $u$ , and  $w(e)$  represents the edge weight for edge  $e$ . Here, we use one of the edge features *road length* as the edge weight  $w(e)$ , such that the estimated eccentricity  $\hat{\epsilon}(v)$  will indicate the maximal traveling distance (in meters) from node  $v$  to its 16-th hop neighbors. Figure 6 shows the distributions of such approximation across different city networks, in which Paris and Shanghai have the most skewed and uniform distributions, respectively. After obtaining the approximations for all nodes, we split them into 10 quantiles as the final node labels.

Then, the computation is at a much cheaper cost of  $\mathcal{O}(|\hat{E}| + |\hat{V}| \log |\hat{V}|)$  using Dijkstra’s algorithm (Dijkstra, 1959), where  $|\hat{V}|$  and  $|\hat{E}|$  are the average number of nodes and edges across all 16-hop ego-networks. The calculation is implemented with `networkx` (Hagberg et al., 2008) on a CPU cluster of 72 Intel Xeon @ 2.3GHz cores, which takes 3, 5, 6, and 23 hours to compute for Paris, Shanghai, L. A. and London, respectively.

## B Experiment Details

### B.1 Baseline Configurations and Resource Consumptions

**Experimental setups.** As discussed in Section 3, we consider two scenarios to show the long-range dependency in our City-Networks:

- Setting the number of layers  $L$  equal to the number of sampling hops  $H$ , and then consider  $L = H \in \{2, 4, 8, 16\}$ .
- Fixing the number of layers at  $L = 16$ , and then vary the number of sampling hops at  $H \in \{2, 4, 8, 16\}$ .

For fair comparison purposes, we set the hidden channel dimension to 32 for all models. Since the number of node features (37) and number of classes (10) are identical across networks, the parameter sizes of the model, as presented in Figure 7, will also remain unchanged on different networks. Note that although some models generally have more parameters than others, with the same number of layers, the parameter sizes are relatively at the same order across all models.

Table 5: Summary of hyper-parameters used for training.

train/valid/test	# epochs	lr	weight decay	dropout	batch size	record window	hidden size
10%/10%/80%	20k	$10^{-3}$	$10^{-5}$	0.2	20k	100	32

The hyperparameters used for training are summarized in Table 5. In particular, we run each model for 20k epochs with a learning rate of  $10^{-3}$  for sufficient training, during which we record the validation accuracy every 100 epochs and save the model at the best validation epoch for final testing. All the scenarios are repeated 5 times and we report their means and standard deviations.

As mentioned in Section 3, we adopt `NeighborLoader` from PyG to sample the supporting subgraph for each node. This method implements the sampling strategy of GraphSAGE (Hamilton et al., 2017), which recursively selects  $[N_1, N_2, \dots, N_H]$  neighbors from a node’s 1st, 2nd, ...,  $H$ -th hop neighborhood. Given the grid-like structure of our city networks, we empirically found that the

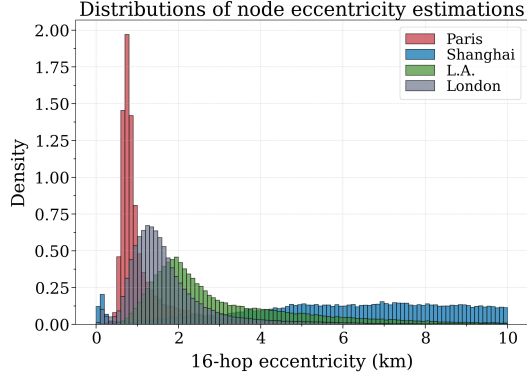


Figure 6: Distribution of the 16-hop eccentricity for all nodes in each of our City-Networks.

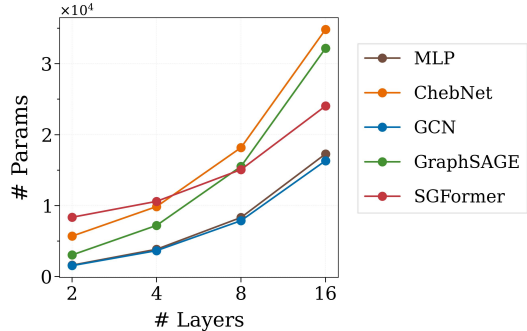


Figure 7: The parameter size of baselines under different number of layers  $L \in [2, 4, 8, 16]$ .

average size of a 16-hop ego-network is typically around  $1k$  nodes, which remains manageable for most GPU devices. Consequently, we set each  $[N_1, N_2, \dots, N_H]$  to  $1k$ , ensuring that the sampled subgraph covers all nodes in the 16-hop neighborhood. Furthermore, we use a `batch_size` of  $20k$  (i.e.,  $20k$  seed nodes) for training and testing. The GPU memory cost and training/testing time are reported in the next section.

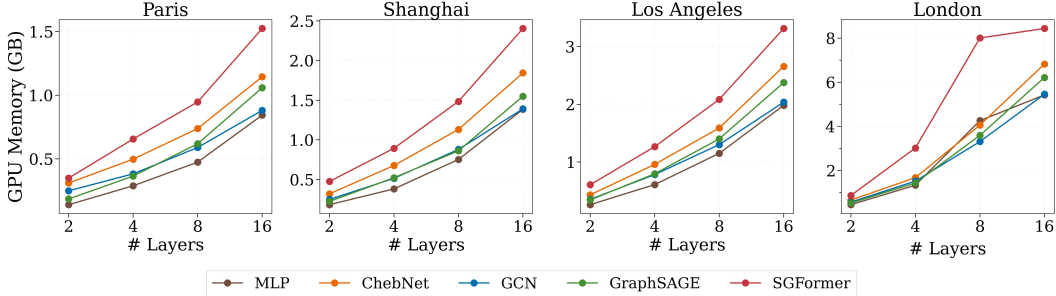


Figure 8: GPU memory consumptions when setting hops  $H$  equals to # layers  $L$  at  $H \in [2, 4, 8, 16]$ .

**Resource monitor.** The experiments are conducted on a cluster of 8 NVIDIA L40 GPUs, each with 48 GB memory. For reference, we monitor the peak GPU memory consumption of models under each setting by running only one job at a time, where we set `batch_size=20k` and vary  $L = H \in [2, 4, 8, 16]$ . The results are shown in Figure 8, in which we can observe that SGFormer, despite having a medium model size among the baselines, occupies the most memory in all cases due to its attention module.

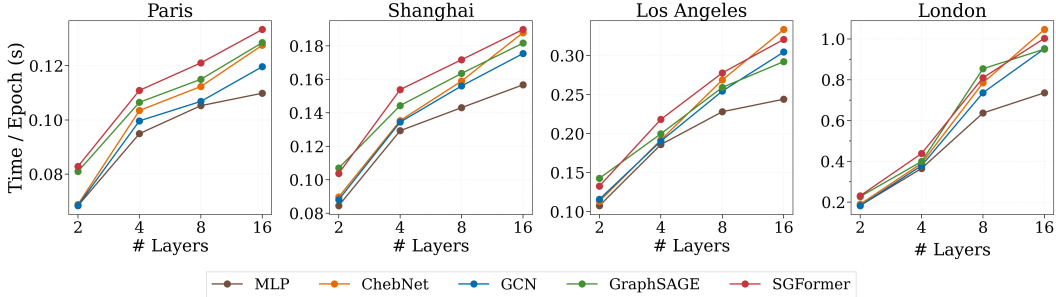


Figure 9: Average training time per epoch with a batch size of  $20k$  seed nodes in NeighborLoader.

Meanwhile, we also record the training/testing clock time per epoch in Figure 9 and Figure 10 respectively. The results suggest that SGFormer generally costs a longer computation time than other GNN baselines at both training and testing, but such difference is insignificant on London. We hypothesize that, since London is at least twice larger than the other networks, it requires more iterations to finish one epoch under the same `batch_size=20k`. This implies that the NeighborLoader needs to sample more ego-networks during training/testing, which is time-consuming when the underlying graph is large.

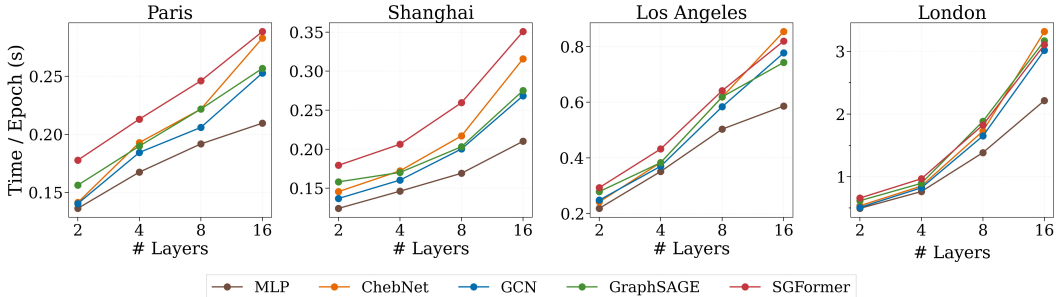


Figure 10: Average testing time per epoch with a batch size of  $20k$  seed nodes in NeighborLoader.

## B.2 Experimental Limitations

**Neighborhood sampling.** As shown in Figure 4, when fixing the number of layers at  $L = 16$ , the trend from  $H = 8$  to  $H = 16$  remains relatively flat, indicating an incremental performance gain. We attribute this phenomenon to the overlapped subgraphs from batched sampling method NeighborLoader, where the ego-networks of different seed nodes often share common supporting nodes. Consequently, if the number of layers  $L$  exceeds  $H$ , the model can capture information from more distant hops beyond  $H$ , rather than being limited to a maximum of  $H$  as expected. This effect is further amplified when using a large batch size (i.e., a large number of seed nodes) or a large number of hops (i.e. a large neighborhood size), as it increases the chance of overlapping ego-networks. Since the node label approximates eccentricity based on its 16-hop neighborhood, there is minimal additional information beyond the 16th hop. As a result, the performance remains similar between these two settings.

**Hyper-parameter selection.** We acknowledge that the results reported in Table 2 may not reflect the models’ optimal performance, as we only considered models with  $L = H = \{2, 4, 8, 16\}$  and a fixed hidden\_size of 32 in our experiments. It is likely that the baselines could achieve better performance with tuned hyperparameters (e.g., learning rate, weight decay, dropout, hidden size, etc.). Nevertheless, we emphasize once again that the primary goal of this work is to analyze the performance trends of each model when varying the number of layers and the number of hops in the sampled neighborhood. This approach incurs a high computational cost on large graphs, which restricts us from conducting extensive hyperparameter optimization, and we leave this potential exploration for future work.

## C Computational Complexity

The computation of  $R$  requires calculating  $T_h(v)$  for  $v \in V$  at  $h \in [0, 1, \dots, H]$ , in which the dominant cost stems from computing the Jacobian matrix. Since the model’s gradient at node  $v$  will be zero for nodes beyond its  $H^{\text{th}}$  hop, we only need to compute the Jacobian within each node’s  $H$ -hop neighborhood. This leads to a computational cost of  $\mathcal{O}(N\bar{N}_H)$ , with  $\bar{N}_H$  being the average size of  $H$ -hop ego-networks on  $\mathcal{G}$ :

$$\bar{N}_H = \frac{1}{N} \sum_{v \in V} |\mathcal{N}_H(v)|, \quad \mathcal{N}_H(v) = \{u \in V \mid d(v, u) \leq H\}, \quad (25)$$

where  $\rho(v, u)$  is the length of shortest path from node  $v$  to node  $u$ . Given the large scale of our city networks, we employ a stochastic approximation that samples  $10k$  nodes to further reduce the computational cost, which can be finished in under 1 hour for all models and networks.

## D Proofs

### D.1 Proofs for Theoretical Results in Section 5

*Proof of Lemma 5.1.* By definition,  $\mathbf{L}_{sym} = \mathbf{I} - \mathbf{S}_{adj}$ . Since both matrices are symmetric, they are diagonalizable with real eigenvalues. Let  $\mathbf{u}$  be an eigenvector of  $\mathbf{L}_{sym}$  with eigenvalue  $\lambda_i(\mathbf{L}_{sym})$ . Then:

$$\mathbf{L}_{sym}\mathbf{u} = \lambda_i(\mathbf{L}_{sym})\mathbf{u} \Rightarrow (\mathbf{I} - \mathbf{S}_{adj})\mathbf{u} = \lambda_i(\mathbf{L}_{sym})\mathbf{u} \Rightarrow \mathbf{S}_{adj}\mathbf{u} = (1 - \lambda_i(\mathbf{L}_{sym}))\mathbf{u}. \quad (26)$$

Therefore,  $\mathbf{u}$  is also an eigenvector of  $\mathbf{S}_{adj}$  with eigenvalue  $1 - \lambda_i(\mathbf{L}_{sym})$ . Since the eigenvalues are ordered in ascending order for  $\mathbf{L}_{sym}$  and the transformation  $1 - \lambda_i$  reverses this ordering, we have  $\lambda_{N+1-i}(\mathbf{S}_{adj}) = 1 - \lambda_i(\mathbf{L}_{sym})$ .  $\square$

*Proof of Proposition 5.2.* Let  $\mathcal{G}'$  be the graph  $\mathcal{G}$  with self-loops added, each having weight  $\gamma > 0$ . If  $\mathcal{G}$  already contains self-loops, their weights are increased by  $\gamma$ . We denote the vertex set of  $\mathcal{G}'$  as  $V$ , with the obvious correspondence to the vertices of  $\mathcal{G}$ . Then  $\mathbf{L}_{sym}^{\mathcal{G}} = \mathbf{I} - \mathbf{D}^{-\frac{1}{2}}\mathbf{A}\mathbf{D}^{-\frac{1}{2}}$  and  $\mathbf{L}_{sym}^{\mathcal{G}'} = \mathbf{I} - (\gamma\mathbf{I} + \mathbf{D})^{-\frac{1}{2}}(\gamma\mathbf{I} + \mathbf{A})(\gamma\mathbf{I} + \mathbf{D})^{-\frac{1}{2}}$ , so proving

$$\lambda_2(\mathbf{L}_{sym}^{\mathcal{G}}) > \lambda_2(\mathbf{L}_{sym}^{\mathcal{G}'}). \quad (27)$$

will prove the proposition. Note that in practice we care about the case where  $\gamma = 1$ . We proceed as follows: we take the eigenfunction on  $\mathcal{G}$  corresponding to  $\lambda_{\mathcal{G}}$ , lift it to  $\mathcal{G}'$ , and show that this yields an upper bound. Using the variational characterisation of eigenvalues in (Chung, 1997, Eq. 1.13) and the fact that edge weights  $w_{\mathcal{G}}(u, v) = w_{\mathcal{G}'}(u, v)$  if  $u \neq v$ , and the degrees of vertices  $d_v^{\mathcal{G}'} = \gamma + d_v^{\mathcal{G}}$ :

$$\lambda_2(\mathbf{L}_{sym}^{\mathcal{G}}) = \inf_{f: \sum_{x \in V} f(x) d_x^{\mathcal{G}} = 0} \frac{\sum_{x \sim y} (f(x) - f(y))^2 w(x, y)}{\sum_{x \in V} f(x)^2 d_x^{\mathcal{G}}} \quad (28)$$

Pick such an  $f$  attaining this infimum (i.e., the eigenvector of  $\mathbf{L}_{sym}^{\mathcal{G}}$  corresponding to  $\lambda_2(\mathbf{L}_{sym}^{\mathcal{G}})$  multiplied by  $\mathbf{D}^{-\frac{1}{2}}$ ). We use this  $f$  to construct a signal  $g$  on  $\mathcal{G}'$ . Let

$$g(x) = f(x) - \frac{\gamma \sum_{x \in V} f(x)}{\sum_{x \in V} d_x^{\mathcal{G}} + \gamma}. \quad (29)$$

That is, we reduce  $f$  by a constant everywhere. We have picked the constant such that

$$\sum_{x \in V} g(x) d_x^{\mathcal{G}'} = \sum_{x \in V} g(x) (d_x^{\mathcal{G}} + \gamma) = 0. \quad (30)$$

Since  $g$  is simply  $f$  shifted by a constant,

$$\forall x, y \in V: g(x) - g(y) = f(x) - f(y). \quad (31)$$

Again, by the variational characterisation of eigenvalues in (Chung, 1997, Eq. 1.13):

$$\lambda_2(\mathbf{L}_{sym}^{\mathcal{G}'}) = \inf_{h: \sum_{x \in V} h(x) d_x^{\mathcal{G}'} = 0} \frac{\sum_{x \sim y} (h(x) - h(y))^2 w(x, y)}{\sum_{x \in V} h(x)^2 d_x^{\mathcal{G}'}} \quad (32)$$

$$\leq \frac{\sum_{x \sim y} (g(x) - g(y))^2 w(x, y)}{\sum_{x \in V} g(x)^2 d_x^{\mathcal{G}'}} = \frac{\sum_{x \sim y} (f(x) - f(y))^2 w(x, y)}{\sum_{x \in V} g(x)^2 d_x^{\mathcal{G}'}} \quad (33)$$

The first inequality holds because  $g$  is in the set  $\{h: \sum_{x \in V} h(x) d_x^{\mathcal{G}'} = 0\}$ , and the infimum serves as a lower bound for the function on any element of that set. The last equality follows from applying (31).

We now show that  $\sum_{x \in V} g(x)^2 d_x^{\mathcal{G}'} > \sum_{x \in V} f(x)^2 d_x^{\mathcal{G}}$ . This will let us bound (33) above by (28). Expanding the definition of  $g$ :

$$\sum_{x \in V} g(x)^2 d_x^{\mathcal{G}'} = \sum_{x \in V} f(x)^2 d_x^{\mathcal{G}'} - 2 \frac{\gamma (\sum_{x \in V} f(x) d_x^{\mathcal{G}'}) (\sum_{x \in V} f(x))}{\sum_{x \in V} d_x^{\mathcal{G}'}} + \frac{\gamma^2 (\sum_{x \in V} f(x))^2}{\sum_{x \in V} d_x^{\mathcal{G}'}} \quad (34)$$

Noting that  $\sum_{x \in V} f(x) d_x^{\mathcal{G}} = 0$  and  $d_x^{\mathcal{G}'} = d_x^{\mathcal{G}} + \gamma$  so  $\sum_{x \in V} f(x) d_x^{\mathcal{G}'} = \gamma \sum_{x \in V} f(x)$ ,

$$\sum_{x \in V} g(x)^2 d_x^{\mathcal{G}'} - \sum_{x \in V} f(x)^2 d_x^{\mathcal{G}} = \gamma \sum_{x \in V} f(x)^2 - 2 \frac{\gamma^2 (\sum_{x \in V} f(x))^2}{\sum_{x \in V} d_x^{\mathcal{G}'}} + \frac{\gamma^2 (\sum_{x \in V} f(x))^2}{\sum_{x \in V} d_x^{\mathcal{G}'}} \quad (35)$$

$$= \gamma \sum_{x \in V} f(x)^2 - \gamma^2 \frac{(\sum_{x \in V} f(x))^2}{\sum_{x \in V} d_x^{\mathcal{G}'}} \quad (36)$$

By the Cauchy-Schwarz inequality on  $f(x)$  and  $\mathbf{1}$ ,

$$\left( \sum_{x \in V} f(x) \right)^2 = \left( \sum_{x \in V} f(x) \cdot 1 \right)^2 \leq \left( \sum_{x \in V} f(x)^2 \right) \left( \sum_{x \in V} 1^2 \right) = n \sum_{x \in V} f(x)^2. \quad (37)$$

Furthermore, as  $\mathcal{G}$  is connected  $\forall x: d_x^{\mathcal{G}} \geq 1$  so  $\sum_{x \in V} d_x^{\mathcal{G}'} > n(1 + \gamma)$ . Therefore:

$$\sum_{x \in V} g(x)^2 d_x^{\mathcal{G}'} - \sum_{x \in V} f(x)^2 d_x^{\mathcal{G}} \geq \frac{\gamma}{n} \left( \sum_{x \in V} f(x)^2 \right) - \gamma^2 \frac{(\sum_{x \in V} f(x))^2}{n(1 + \gamma)} \quad (38)$$

$$= \frac{(\sum_{x \in V} f(x))^2}{n} \left( \gamma - \frac{\gamma^2}{1 + \gamma} \right) \quad (39)$$

$$= \frac{(\sum_{x \in V} f(x))^2}{n} \left( \frac{\gamma}{1 + \gamma} \right) \quad (40)$$

$$> 0. \quad (41)$$

Based on which we conclude that  $\sum_{x \in V} g(x)^2 d_x^{\mathcal{G}'} > \sum_{x \in V} f(x)^2 d_x^{\mathcal{G}}$ , and so by (28) and (33):

$$\lambda_2(\mathbf{L}_{sym}^{\mathcal{G}'}) \leq \frac{\sum_{x \sim y} (f(x) - f(y))^2 w(x, y)}{\sum_{x \in V} g(x)^2 d_x^{\mathcal{G}'}} \quad (42)$$

$$< \frac{\sum_{x \sim y} (f(x) - f(y))^2 w(x, y)}{\sum_{x \in V} f(x)^2 d_x^{\mathcal{G}}} = \lambda_2(\mathbf{L}_{sym}^{\mathcal{G}}). \quad (43)$$

Hence,  $\lambda_2(\mathbf{L}_{sym}^{\mathcal{G}}) > \lambda_2(\mathbf{L}_{sym}^{\mathcal{G}'})$  and by (27), the proof is complete.  $\square$

*Proof for Theorem 5.3.* Given Proposition 5.2 and the correspondence between the eigenvalues of  $\mathbf{S}_{adj}$  and  $\mathbf{L}_{sym}^{\mathcal{G}}$ , the result follows immediately from (Chung, 1997, Lemma 1.14).  $\square$

## D.2 Proofs for Theoretical Results in Section 6

*Monotonicity of the Softmax function.* Consider the derivative of the  $i$ -th softmax probability with respect to its corresponding logit:

$$\frac{\partial p_i}{\partial z_i} = \frac{\partial}{\partial z_i} \left( \frac{\exp(z_i)}{\sum_j \exp(z_j)} \right) = \frac{\exp(z_i) \sum_j \exp(z_j) - \exp(z_i) \exp(z_i)}{(\sum_j \exp(z_j))^2} = p_i(1 - p_i) \quad (44)$$

Observe that:  $p_i(1 - p_i) > 0$  for  $0 < p_i < 1$  and  $\frac{\partial p_i}{\partial z_i} \rightarrow 0$  as  $p_i \rightarrow 0$  or  $p_i \rightarrow 1$ . For  $j \neq i$ :

$$\frac{\partial p_i}{\partial z_j} = \frac{\partial}{\partial z_j} \left( \frac{\exp(z_i)}{\sum_h \exp(z_h)} \right) = -\frac{\exp(z_i) \exp(z_j)}{(\sum_h \exp(z_h))^2} = -p_i p_j \quad (45)$$

This proves that the softmax probabilities increase with their corresponding logits and decrease with other logits.  $\square$

*Proof of Proposition 6.1.* Let  $f : \mathbb{R}^D \rightarrow \mathbb{R}$  be a differentiable function with  $f'(\mathbf{X}) \neq 0$  at some  $\mathbf{X}$ . For simplicity set  $D = 1$  and let  $\mathbf{X} = x$  (scalar case). Define a model by

$$k(x) = k_1(x) + k_2(x), \quad (46)$$

$$k_1(x) = f(x), \quad (47)$$

$$k_2 = -f(x). \quad (48)$$

We first observe that for any  $x$ ,

$$k(x) = f(x) - f(x) = 0. \quad (49)$$

By differentiability, the derivative is

$$k'(x) = k_1'(x) + k_2'(x) = f'(x) - f'(x) = 0. \quad (50)$$

Thus, a perturbation in  $x$  has no net effect (i.e., zero influence) on  $k(x)$ . However, we note that there are two branches:  $k_1'(x)$  with derivative  $f'(x)$ ,  $k_2'(x)$  with derivative  $-f'(x)$ . If we assess sensitivity by taking the absolute value of each derivative (i.e., the magnitude of each influence), we obtain

$$|f'(x)| \quad \text{and} \quad |-f'(x)| = |f'(x)|, \quad (51)$$

so that the total influence would be

$$|k_1'(x)| + |k_2'(x)| = 2|f'(x)|. \quad (52)$$

$\square$

**Definition D.1** (Smooth Hypersurface in  $\mathbb{R}^D$ ). A hypersurface in  $\mathbb{R}^D$  is a subset defined locally as the zero set of a continuously differentiable function  $f : \mathbb{R}^D \rightarrow \mathbb{R}$  such that the gradient  $\nabla f$  is nonzero at almost every point where  $f = 0$ . That is, if we have an equation of the form  $f(\boldsymbol{\theta}) = 0$ , where  $\boldsymbol{\theta}$  is a vector of parameters, and if  $\nabla f(\boldsymbol{\theta}) \neq 0$  generically, then  $f = 0$  defines a (locally)  $(D - 1)$ -dimensional manifold, which is a hypersurface.

*Proof of Theorem 6.3.* For exact cancellation to hold assuming  $\oplus = \sum$ , the following sum must be identically zero while the individual terms remain non-zero. Since  $\psi$  and  $\phi$  are differentiable and parameterized by  $\theta$ , each Jacobian term is a smooth function of  $\theta$ . The equation:

$$f(\theta) = \sum_{u \in \mathcal{N}(v)} \frac{\partial \psi(\mathbf{X}_v^{(l)}, \mathbf{X}_u^{(l)})}{\partial \mathbf{X}_u^{(l)}} = 0, \quad (53)$$

defines a level set of smooth functions, a hypersurface (or a set of lower-dimensional submanifolds) in parameter space. The solution set of a nontrivial smooth function has Lebesgue measure zero unless it is identically zero across all  $\theta$ , which is not the case here. Furthermore, since  $\theta$  is drawn from an absolutely continuous distribution (such as Gaussian or uniform), the probability of exactly selecting a parameter that lies on this hypersurface is zero at initialization. Thus, exact cancellation of Jacobian contributions is an event of measure zero in the space of our idealized single-layer MPNN: this can naturally be extended to multiple layers. Note that in this proof we have assumed the Jacobian sum is not identically zero by construction, unlike in Proposition 6.1 where the function was explicitly constructed to ensure cancellation.  $\square$

*Proof of Lemma 6.7.* Since  $\mathcal{G}$  is grid-like in  $D$  dimensions, its structure mimics that of  $\mathbb{Z}^D$ . In  $\mathbb{R}^D$ , the volume of a ball of radius  $h$  scales as  $h^D$  (recall the volume of a sphere in  $\mathbb{R}^3$  is  $\frac{4}{3}\pi h^3$ ). Let

$$B_h(v) = \{u \in V : \rho(v, u) \leq h\}, \quad (54)$$

denote the ball of radius  $h$  centered at  $v$ . Then for large  $h$  (asymptotic bound),

$$|B_h(v)| = \Theta(h^D). \quad (55)$$

Since the  $h$ -hop neighborhood is the set difference

$$\mathcal{N}_h(v) = B_h(v) \setminus B_{h-1}(v). \quad (56)$$

This effectively means that the size of  $\mathcal{N}_h(v)$  is approximately the difference between the volume of two consecutive balls:

$$|\mathcal{N}_h(v)| = |B_h(v)| - |B_{h-1}(v)|. \quad (57)$$

A standard asymptotic argument implies

$$|\mathcal{N}_h(v)| = \Theta(h^{D-1}), \quad (58)$$

since we can approximate the aforementioned difference via:

$$|B_h(v)| - |B_{h-1}(v)| = \mathfrak{C}h^D - \mathfrak{C}(h-1)^D \approx \mathfrak{C}h^D - \mathfrak{C}(h^D - Dh^{D-1}) = \mathfrak{C}Dh^{D-1}, \quad (59)$$

using the binomial expansion and assuming large  $h$  (we are concerned with long-range interactions), where the leading order term dominates. Intuitively, this corresponds to the *surface growth* of the ball, which in  $\mathbb{R}^D$  scales as  $h^{D-1}$  (the area of a sphere in  $\mathbb{R}^3$  is  $4\pi h^2$ ). Thus, there exist constants  $\mathfrak{C}_1, \mathfrak{C}_2 > 0$  and an integer  $h_0$  such that for all  $h \geq h_0$ ,

$$\mathfrak{C}_1 h^{D-1} \leq |\mathcal{N}_h(v)| \leq \mathfrak{C}_2 h^{D-1}. \quad (60)$$

$\square$

*Proof of Theorem 6.8.* Assume that within  $\mathcal{N}_h(v)$  there is a unique node  $u^*$  with a strong influence  $I(v, u^*) = I^* > 0$  and that for all other nodes  $u \in \mathcal{N}_h(v) \setminus \{u^*\}$ , the influence  $I(v, u)$  is negligible ( $\Delta \approx 0$ ). Then:

The *total* (or *sum*) influence is

$$I_{\text{sum}}(v, h) = \sum_{u \in \mathcal{N}_h(v)} I(v, u) \geq I(v, u^*) = I^*. \quad (61)$$

The *mean* influence is given by

$$I_{\text{mean}}(v, h) = \frac{1}{|\mathcal{N}_h(v)|} \sum_{u \in \mathcal{N}_h(v)} I(v, u) = \frac{1}{|\mathcal{N}_h(v)|} (I^* + \sum_{u \in \mathcal{N}_h(v) | u \neq u^*} I(v, u)) = \frac{I^* + \Delta}{|\mathcal{N}_h(v)|}. \quad (62)$$

Using the lower bound on  $|\mathcal{N}_h(v)|$ ,

$$I_{\text{mean}}(v, h) \leq \frac{I^* + \Delta}{\mathfrak{C}_1 h^{D-1}}. \quad (63)$$

Since  $h^{D-1} \rightarrow \infty$  as  $h \rightarrow \infty$  for  $D \geq 2$ , it follows that

$$I_{\text{mean}}(v, h) \rightarrow 0, \quad (64)$$

while  $I_{\text{sum}}(v, h) \geq I^*$  remains non-vanishing.  $\square$

*Proof of Corollary 6.9.* For a planar graph that is grid-like (for example, a two-dimensional lattice), set  $D = 2$ . Then,  $|\mathcal{N}_h(v)| = \Theta(h^{2-1}) = \Theta(h)$ . Repeating the same argument as above: the total influence satisfies  $I_{\text{sum}}(v, h) \geq I^*$ . The mean influence is bounded by  $I_{\text{mean}}(v, h) \leq \frac{I^*}{|\mathcal{N}_h(v)|} \leq \frac{I^*}{\mathfrak{C}_1 h}$ . Hence, as  $h \rightarrow \infty$ ,  $I_{\text{mean}}(v, h) \rightarrow 0$ , which demonstrates that for a planar graph the dilution of the mean aggregated influence occurs at a rate proportional to  $1/h$ .  $\square$

*Proof of Corollary 6.10.* Since  $\mathcal{G}$  is grid-like in  $D$  dimensions, the size of the aggregated  $h$ -hop neighborhood (the ball) grows as  $|B_h(v)| = \Theta(h^D)$ . Assuming that only one node  $u^*$  in  $B_h(v)$  has a significant influence  $I^*$  while the influence of all other nodes is negligible, the total (or sum) influence satisfies  $I_{\text{sum}}^B(v, h) \geq I^*$ . Thus, the mean influence over  $B_h(v)$  is  $I_{\text{mean}}^B(v, h) \leq \frac{I^*}{\Theta(h^D)}$ . That is, there exists a constant  $\mathfrak{C}' > 0$  such that  $I_{\text{mean}}^B(v, h) \leq \frac{I^*}{\mathfrak{C}' h^D}$ . Since  $h^D \rightarrow \infty$  as  $h \rightarrow \infty$  for  $D \geq 1$ , it follows that  $I_{\text{mean}}^B(v, h) \rightarrow 0$ .  $\square$

*Proof of Corollary 6.11.* For any node  $v \in V$ , by the distinguished node assumption (reused from Theorem 6.8) there is at least one  $u^* \in \mathcal{N}_h(v)$  with

$$I(v, u^*) \geq I^*. \quad (65)$$

Since the total influence is a sum over nonnegative contributions, it follows that

$$T_h(v) = \sum_{u \in \mathcal{N}_h(v)} I(v, u) \geq I(v, u^*) \geq I^*. \quad (66)$$

Averaging over all nodes in  $V$ ,

$$\bar{T}_h = \frac{1}{|V|} \sum_{v \in V} T_h(v) \geq \frac{1}{|V|} \sum_{v \in V} I^* = I^*. \quad (67)$$

This bound is independent of the size  $|\mathcal{N}_h(v)|$  of the  $h$ -hop neighborhood and hence remains valid even as  $|\mathcal{N}_h(v)|$  (or the overall number of nodes) tends to infinity.

$$\bar{T}_h = \frac{1}{|V|} \sum_{v \in V} T_h(v) \geq I^*, \quad \forall h. \quad (68)$$

$\square$